

Symmetry controlled single spin cycloid switching in multiferroic BiFeO₃

Pratap Pal,^{1,†} Jonathon L. Schad,^{1,†} Anuradha M. Vibhakar,² Shashank Kumar Ojha,³ Gi-Yeop Kim,⁴ Saurav Shenoy,⁵ Fei Xue,⁵ Mark S. Rzchowski,⁶ A. Bombardi,² Roger D. Johnson,^{2,7} Si-Young Choi,⁴ Long-Qing Chen,⁵ Ramamoorthy Ramesh,^{3,7,8,9,10,11} Paolo G. Radaelli,¹² and Chang-Beom Eom^{1*}

¹Department of Materials Science and Engineering, University of Wisconsin-Madison, Wisconsin 53706, USA.

²Diamond Light Source Ltd, Harwell Science and Innovation Campus, Didcot, OX11 0DE, United Kingdom.

³Rice Advanced Materials Institute, Rice University, Houston, TX, 77005, USA.

⁴Department of Materials Science and Engineering Pohang University of Science and Technology, Pohang, Gyeongbuk 37673, Republic of Korea.

⁵Department of Materials Science and Engineering, The Pennsylvania State University, University Park, Pennsylvania 16802, USA.

⁶Department of Physics, University of Wisconsin-Madison, Wisconsin 53706, USA.

⁷Department of Physics and Astronomy, University College London, London, WC1E 6BT, United Kingdom.

⁷Materials Sciences Division, Lawrence Berkeley National Laboratory, Berkeley, CA, 94720, USA.

⁸Department of Materials Science and Engineering, University of California, Berkeley, CA, 94720, USA

⁹Department of Materials Science and NanoEngineering, Rice University, Houston, TX, 77005, USA

¹⁰Departments of Chemistry and Physics and Astronomy, Rice University, Houston, TX, 77005, USA

¹¹Department of Physics, University of California, Berkeley, CA, 94720, USA

¹²Clarendon Laboratory, Department of Physics, University of Oxford, Oxford OX1 3PU, United Kingdom.

*Corresponding author: ceom@wisc.edu

†These authors contributed equally.

Abstract

The single variant spin cycloid and associated antiferromagnetic order in multiferroic BiFeO₃ can provide a direct and predictable magnetoelectric coupling to ferroelectric order for deterministic switching, and also a key to fundamental understanding of spin transport and magnon-based applications in the system. (111) oriented BiFeO₃ supplies an easy magnetic plane for the spin cycloid, but despite previous efforts, achieving deterministic switching of the single spin cycloid over multiple cycles remains challenging due to the presence of multiple spin cycloid domains in the (111) plane. Here we show that anisotropic in-plane strain engineering can stabilize a single antiferromagnetic domain and provide robust, deterministic switching. We grow BiFeO₃ on orthorhombic NdGaO₃ (011)_o [(111)_{pc}] substrates, breaking the spin cycloid degeneracy and by imposing a uniaxial strain in the (111) plane. This stabilization is confirmed through direct imaging with scanning NV microscopy and non-resonant X-ray diffraction. Remarkably, we achieved deterministic and non-volatile 180° switching of ferroelectric and associated antiferromagnetic domains over 1,000 cycles, significantly outperforming existing approaches. Our findings underscore that anisotropic strain engineering opens up exciting possibilities for (111)_{pc} monodomain BiFeO₃ in potential magnetoelectric and emerging magnonic applications.

Introduction

Multiferroic materials with significant magnetoelectric coupling have shown considerable technological potential, enabling energy-efficient control of magnetism through an electric field.¹⁻⁴ Among these, BiFeO₃ (BFO) is the most extensively studied single-phase room-temperature magnetoelectric multiferroic⁵⁻⁷, with coupled antiferromagnetic and ferroelectric orders; however, its optimal use is constrained by complex domain structures⁸ of ferroelectric and associated ferroelastic distortions, of unit cell periodic antiferromagnetic order and associated long-wavelength spin cycloid. BFO exhibits a rhombohedral (R3c) crystal symmetry, resulting in four possible ferroelastic domains (Fig. S1) with the spontaneous distortion along each of the [111]_{pc} body diagonals (“_{pc}” indicates a pseudo-cubic basis)⁹. Each ferroelastic domain can contain two ferroelectric variants, r_i^+ and r_i^- along the $\pm[111]_{pc}$ directions¹⁰. Furthermore, each ferroelectric domain is coupled to three equivalent non-collinear antiferromagnetic domains (Fig. S1b) hosting type I spin cycloid, characterized by propagation vectors $\mathbf{k}_1 = [-1, 1, 0]_{pc}$, $\mathbf{k}_2 = [0, -1, 1]_{pc}$, and $\mathbf{k}_3 = [1, 0, -1]_{pc}$ ^{11,12}. This total of 24 domain variants (4 ferroelastic \times 2 ferroelectric \times 3 antiferromagnetic) complicates the study of ferroelectric switching and poses significant challenges for retention and reliability. Also leakage currents associated with ferroelectric domain walls¹³ is detrimental to deterministic switching^{4,14}. Multiple antiferromagnetic domains hinder one-to-one coupling with a top ferromagnetic layer for electric field control of magnetism^{15,16}. Therefore, achieving a single-domain BFO thin film is desirable for electric-field-controlled magnetoelectric device applications. The ongoing challenge is how to effectively control these domain populations to attain a uniform single-domain state.

Although (001)_{pc} BFO single ferroelastic-ferroelectric domains have been achieved with a substrate miscut towards the in-plane [110] direction⁸, controlling antiferromagnetic domains remains challenging as they respond only weakly to external perturbations¹⁷. Additionally, in this orientation, the ferroelectric polarization undergoes a 71° switching accompanied by an associated ferroelastic domain switching, so that mechanical stress at the boundary leads to destabilization and back-switching of the switched region¹⁸ and loss of retention of ferroelectric switching in (001)_{pc} BFO. This has been addressed with (111)_{pc} oriented BiFeO₃. In this orientation, no ferroelastic deformation upon switching is expected^{19,20}, thus stabilizing a single ferroelastic domain without any miscut²¹. In addition, 180° reversal of the weak local magnetization (which changes sign with the same periodicity as the cycloid of the antiferromagnetic domain) is predicted to be achievable in (111)_{pc} BFO²², whereas it is limited in the (001) configuration^{16,23-25}. These factors position (111)_{pc} BFO as an ideal platform for integration into magnetoelectric devices, but the three degenerate antiferromagnetic domains (Figs. 1a and b) lead to significant disadvantages for deterministic magnetic switching^{26,27}. And films in this orientation have been plagued by electrical breakdown and polarization fatigue attributed to the non-deterministic multi-path ferroelectric switching process arising from multiple domains (Figs. 1d and e)^{19,21}.

Here we show that substrate interactions that break a crucial symmetry can eliminate this antiferromagnetic domain degeneracy and provide deterministic switching. (111) BFO is most easily grown on a symmetry-preserving substrate such as SrTiO₃, which preserves and stabilizes the three equivalent monoclinic domains (M1, M2 and M3), inter-related by the *pseudo*-rhombohedral symmetry²¹. These three structural domains have a one-to-one relationship with cycloidal magnetic domains characterized by propagation vectors \mathbf{k}_1 , \mathbf{k}_2 , and \mathbf{k}_3 , respectively^{26,28}. We also demonstrate that anisotropic compressive strain (Fig. 1c) rather than the symmetric in-plane strain provided by (111) SrTiO₃ substrate (Fig. 1b) lifts the degeneracy of these monoclinic structural domains and selects a specific variant of the antiferromagnetic

spin cycloid. We employ NdGaO_3 $(011)_o$ oriented (equivalent to $(111)_{pc}$) orthorhombic substrates (“ o ” indicates an orthorhombic basis) to generate the anisotropic in-plane strain. Using real-space NV microscopy imaging and non-resonant X-ray magnetic scattering techniques, we show that this approach lifts the degeneracy of the monoclinic structural domains unlike the (111) SrTiO_3 substrate, where symmetric in-plane strain maintains this degeneracy and stabilizes a single variant of the spin cycloid, along with single ferroelectric and ferroelastic domains. Most importantly, our films exhibit deterministic switching that is reliable and non-volatile over one hundred thousand cycles, due to the single preferred ferroelectric switching path (Fig. 1f). This anisotropic strain design demonstrates monodomain $(111)_{pc}$ BiFeO_3 which circumvents major challenges of reliable and nonvolatile electric field writing for potential magnetoelectric device applications.

Results and Discussions

Anisotropic strain engineering of Epitaxial $(111)_{pc}$ BiFeO_3

We used phase field calculations to make a detailed probe of the role of anisotropic strain. These calculations were performed considering the total free energy of an inhomogeneous system that includes ferroelectric polarization distribution, oxygen octahedral tilt, and antiferromagnetic order. The polarization is coupled to the antiferromagnetic order \vec{L} through the Lifshitz invariant, which is responsible for the incommensurate spin cycloid²⁹. Figure 1b shows the calculated system free energy of an isotropic BFO film on SrTiO_3 substrate as a function of spin cycloid propagation wavevector, with Fig. 1c showing the result for anisotropic compressive strain imposed by a NdGaO_3 substrate. This clearly illustrates that while there are three degenerate antiferromagnetic domains in the case of isotropic strain, anisotropic strain lifts the degeneracy, stabilizing a single variant of the antiferromagnetic spin cycloid.

We grew high-quality $(111)_{pc}$ BiFeO_3 epitaxial thin films on both orthorhombic NdGaO_3 $(011)_o$ and (111) SrTiO_3 substrates (Figs. S2 and S3) with epitaxial SrRuO_3 metallic oxide bottom electrode by using off-axis magnetron sputtering. NdGaO_3 $(011)_o$ is expected to impart anisotropic compressive in-plane strain of approximately 2.5% along $[1-10]_{pc}$ direction and 2.0% along the $[11-2]_{pc}$ directions, in contrast to the isotropic compressive in-plane strain in the case of SrTiO_3 substrates³⁰. To understand the impact of the orthorhombic substrate on the symmetry of these BiFeO_3 films, we performed reciprocal space mapping (RSM) along different azimuthal directions (Fig. S5). The results indicate that BiFeO_3 films on SrTiO_3 maintain a macroscopically high symmetry when averaging over all domains, whereas those grown on NdGaO_3 demonstrate reduced in-plane symmetry at all length scales, as hypothesized. This reduction of the in-plane symmetry, even in relaxed BiFeO_3 films, can facilitate the formation of a single antiferromagnetic domain, consistent with our thermodynamic analysis.

We examined the microstructure of the BiFeO_3 film on NdGaO_3 with scanning transmission electron microscopy (STEM) to gain direct insight into the in-plane anisotropic strain. A low-magnification cross-sectional STEM image (Fig. S6a) reveals a BiFeO_3 film with a single ferroelastic domain throughout its entire thickness. Atomic resolution high-angle annular dark field (HAADF) images further confirm the excellent epitaxial arrangement and atomically sharp interfaces (Figs. 2b and c),³¹ despite the large lattice mismatch between the BiFeO_3 film and NdGaO_3 substrate. To quantitatively assess the anisotropic lattice strain, we performed STEM strain mapping analyses (Figs. 2d and e) along the A ($[1-10]_{pc}$) and B ($[11-2]_{pc}$) directions in the BiFeO_3 layer near the interfaces. The line profile results from the strain maps show that ϵ_{AA} value (2.75 %) in the BiFeO_3 region is higher than ϵ_{BB} value (2.2 %), indicating a larger compressive

strain state along the A ($[1-10]_{pc}$) direction compared to the B ($[11-2]_{pc}$) direction, as illustrated in Fig. 2a.. Therefore, BiFeO₃ on NdGaO₃ provides a novel platform with anisotropic compressive strain to test our hypothesis regarding antiferromagnetic domain control.

Realization of single variant spin cycloid in monodomain (111) BiFeO₃ thin films

To investigate the nature of the ferroelastic domain, we employed synchrotron X-ray diffraction for reciprocal space mapping (RSM) scans around the out-of-plane $(111)_{pc}$ peak. Fig. S13a clearly indicates the presence of only the r_1 domain,²¹ with no signatures of other minority domains in the BiFeO₃ film grown on NdGaO₃ substrates. Piezoforce microscopy (PFM) images show a consistent downward-directed ferroelectric polarization state in the as-grown films, attributed to the screening effect of the SrRuO₃ bottom electrode (Fig. S7).

While probing the ferroelastic and ferroelectric domain structures is relatively straightforward, directly mapping the antiferromagnetic domains is more challenging, as it is limited to detecting the weak, spatially alternating magnetization that arises from a Dzyaloshinskii–Moriya interaction-driven orthogonal spin-density wave^{11,32}. In this context, scanning NV (nitrogen-vacancy) diamond microscopy has emerged as a promising tool for mapping the surface stray magnetic field with nanoscale resolution (Fig. 3a)^{11,33–35}. Fig. 3b shows a typical dual iso- B NV image of BiFeO₃ film on SrTiO₃, revealing a continuously rotating pattern of spin-cycloid on the $(111)_{pc}$ surface in which the spin cycloid propagates in various directions³⁶. Since the BiFeO₃ film is isotropically strained on symmetric cubic SrTiO₃, the degeneracy of the antiferromagnetic domains is preserved, resulting in this intricate magnetic pattern with multiple k -vectors, as evident from the first Fourier transform (FFT) image (inset to Fig. 3b)^{26,37,38}. Interestingly, this magnetic texture on the (111) surface resembles a glassy labyrinthine pattern³⁹, which can be qualitatively understood by considering the (111) plane as a magnetic easy plane.

In contrast, NV scan of the BiFeO₃ film grown on $(011)_o$ NdGaO₃ reveals a well-ordered periodic pattern of spin-cycloid, as shown in Fig. 3c. This pattern propagates in a definite direction (along $[1-10] \parallel a_o$ direction) on the $(111)_{pc}$ surface³⁶. Since dual iso- B signal is semiquantitative, we also conducted measurements in full- B mode⁴⁰ (see Methods) which directly quantifies the magnitude of the local stray magnetic field, and found a similar ordered variation in the local magnetic field arising from the spin cycloids (Fig. S10). These NV scanning images highlight the presence of multiple magnetic propagation vectors in case of SrTiO₃, while the clear spin-cycloid observed for NdGaO₃ indicated the stabilization of an antiferromagnetic monodomain state with a single propagation vector^{36,41,42}, which is highly favorable for direct coupling to a device.

Understanding of single variant spin cycloid stabilization

While the stabilization of single ferroelastic and ferroelectric domains is well understood, the stabilization of antiferromagnetic monodomains (single variant spin cycloid) is less straightforward^{8,21,36}. To explore factors that stabilize a single antiferromagnetic domain in BiFeO₃ on $(011)_o$ NdGaO₃ (Fig. 3c), we conducted thermodynamic phase-field simulations implementing an anisotropic strain imposed by NdGaO₃. Notably, our results reveal the stabilization of only one type of antiferromagnetic domain characterized by a distinct spin-cycloid propagation direction (Figs. 3d and 3e) for orthorhombic NdGaO₃

(011)_o, consistent with experimental observations. Thus, the calculations that relaxed to this monodomain antiferromagnetic state after initiation from a random state (Fig. S19) indicate magnetoelastic coupling as the strong driving force arising from the anisotropic strain. The corresponding regular modulation of the out-of-plane antiferromagnetic \vec{L} -vector is also evident (Fig. 3e). A representative line section profile from the NV scan image demonstrates that the periodicity of the stray magnetic field of ~ 62 nm that closely matches the periodicity predicted by thermodynamic calculations (Fig. 3f). This highlights the critical role of anisotropic strain in the (111)_{pc} plane, which facilitates the seeding of the monodomain antiferromagnetic state. We propose that this monodomain state nucleates along a specific direction, resulting in coherent spin-cycloid propagation throughout the film. Our combined experimental and theoretical results support the notion of strong magnetoelastic coupling between structural and magnetic orders in BiFeO₃⁴³. Interestingly, a closer examination of the NV images reveals local interruptions in cycloid propagation (Fig. 3g), suggesting topological defects, which are even more pronounced in films on SrTiO₃ (Fig. 3b).

Deterministic and non-volatile switching of all multiferroic orders

To establish the connection of complete monodomain states with stability and robustness under electric field switching we combined PFM, NV imaging, and non-resonant X-ray magnetic scattering. First, we used a PFM tip to switch the ferroelectric domains. A clear hysteresis of the vertical piezoresponse is observed, indicating 180° polarization switching from down to up (Fig. S8). Similarly, a box-in-a-box pattern (Fig. 4a) was written with the PFM tip, where the first inside box represents a complete reversal of the ferroelectric domains.

The corresponding NV scan image (Fig. S10) shows a strong electric field response, with switching from down to up resulting in non-cycloidal, uniform local surface magnetization, potentially attributed to flexoelectric effects⁴⁴. Notably, after completing one full cycle of switching (down-up-down) a robust single variant of the spin-cycloid (Fig. 4b) is restored, necessary for magnetoelectric device applications.

To investigate switching at times scales than the relatively slow PFM switching process, we applied a square electric field pulse to switch the ferroelectric polarization back and forth by 180° over a hundred thousand cycles. While the polarization of BiFeO₃ on SrTiO₃ degrades after just a few thousand cycles¹⁹, we found that the polarization on NdGaO₃ remains robust with negligible reduction (Fig. 4c). This polarization fatigue-free response from the (111)_{pc} monodomain BiFeO₃ is a key advancement for deterministic information writing in device applications. Importantly, this deterministic switching (down to up) in (111)_{pc} monodomain BiFeO₃ is non-volatile and is maintained over thousands of hours (Fig. S9), unlike (001) monodomain BiFeO₃¹⁸.

To further investigate the effect of electric field switching on antiferromagnetic domain stability, we conducted non-resonant X-ray magnetic scattering (NXMS) measurements using synchrotron X-ray diffraction, as shown in Fig. 4d. These measurements focused on satellites of the (009)_h reflection (“*h*” denotes the hexagonal setting), which correspond to long-range incommensurate magnetic ordering^{21,26}. A 200 μm × 50 μm area of the as grown virgin sample was used for reciprocal-space mapping. The *i*th magnetic domain is associated with two satellite peaks at positions (009)_h ± **k**_{*i*}. The BiFeO₃ film grown on NdGaO₃ shows only one pair of magnetic satellite peaks at (009)_h ± **k**₃ (aligned along the [100]_o direction of the substrate) in the as grown state (Fig. 4e), unlike what was observed on SrTiO₃²¹, confirming the presence of a single antiferromagnetic cycloidal domain^{21,26}, associated with the major **r**₁ ferroelastic domain. The

lack of diffuse intensity between the two magnetic satellite peaks indicates a coherent magnetic structure throughout the film, consistent with NV scanning images.

We then conducted a similar reciprocal-space mapping on a 75 μm by 50 μm area of a region of the sample test structure (Fig. S12) that had been electrically switched 1,000 times and left in the up-polarization state. Interestingly, the same magnetic satellite peaks were observed, confirming the presence of a single antiferromagnetic cycloidal domain in both the as-grown (down \vec{P}) and switched (up \vec{P}) states of the film. The associated ferroelastic domain also remains, on average greater than 99.0% a single variant (Fig. S13b) after electric field switching. This represents a major advance in creating BiFeO₃ thin films that maintain a single domain even after extensive electrical switching, underscoring how interfacial strain (which is overall relaxed in the 1 μm thick film) manipulation between substrate and film can yield robust domain structures in thin films.

Mechanism behind robust deterministic switching

We now explore additional key aspects that make BiFeO₃ grown on NdGaO₃ particularly special for optimizing robust single-domain multiferroic order. In response to an out-of-plane applied electric field, the 180° polarization switching in BiFeO₃ (111) can involve intermediate stages, such as an initial 71° switching followed by a 109° switching (Fig. 1d)⁴⁵. Previously, it was observed that this 71° switching could occur through multiple pathways when BiFeO₃ was grown on SrTiO₃ (Fig. 1e), leading to head-to-head (or tail-to-tail) charge domain walls, which caused polarization fatigue^{21,45}. In contrast, when BiFeO₃ is grown on an orthorhombic NdGaO₃ substrate, the symmetry of the (111)_{pc} plane is broken due to anisotropic compressive strain, resulting in a preferred single-path switching mechanism, as also indicated in our phase field simulations shown in Fig. S20 (Fig. 1f and Fig. S17). This eliminates the formation of charged domain walls, providing a fatigue-free ferroelectric switching response over one hundred thousand cycles.

Furthermore, NdGaO₃ imposes anisotropic compressive strain along both in-plane directions (as shown in Supplementary Section XVI and Fig. S16), in contrast to alternative anisotropy strain, such as that imposed by TbScO₃ where both tensile and compressive strains are present. While TbScO₃ has been shown to stabilize a single-domain (111) BiFeO₃²³, it loses about 50% of its stability after electrical switching due to the formation of minority domains in the direction of tensile strain²³. In the present case of NdGaO₃, the compressive strain along both directions plays a crucial role in stabilizing robust, single-domain (111)_{pc} BiFeO₃ thin films, marking a significant advancement in the field.

Conclusions and Outlook

We have demonstrated the stabilization of robust monodomain states (single ferroelastic, ferroelectric, and antiferromagnetic) and deterministic switching in (111)_{pc} BiFeO₃ thin films through anisotropic compressive strain and symmetry engineering. Notably, we achieved fatigue-free, deterministic electric field switching sustained over one hundred thousand cycles. This electric field writing is non-volatile, retaining information for thousands of hours—an essential feature for electric field-based memory applications.

Since the ferroelectric polarization (P) is linearly coupled to magnetic polarity ($\lambda = r_{ij} \times (S_i \times S_j)$),

where S_i and S_j are nearest-neighbor spins, and r_{ij} is a vector connecting spins i and j), switching P with an applied electric field is expected to induce a corresponding reversal of the cycloidal polarity^{28,41}. This opens the possibility of achieving 180° electric field switching of the magnetic moment in a thin ferromagnetic overlayer (e.g., Co¹⁶) atop (111)_{pc} monodomain BiFeO₃ through one-to-one exchange coupling (between single-cycloid antiferromagnetism and top ferromagnetism), an exciting direction for future research.

Additionally, recent advances in non-local spin transport via low-energy magnon modes show promise for the development of magnonic devices^{42,46}. In this context, (111)_{pc} monodomain BiFeO₃ thin films offer a compelling platform for unconventional, anisotropic, and highly efficient spin transport (as they lie in the magnetic easy plane, unlike the (001) configuration) in non-local devices. Thus, our design principle represents a significant step toward optimizing single ferroelectric and antiferromagnetic domains in BiFeO₃, advancing the development of low-power, electric field-switchable memory devices.

Methods

Thin films sample growth, and characterization.

(111)_{pc} monodomain BiFeO₃ thin films were grown on cubic SrTiO₃ (111) and orthorhombic NdGaO₃ (011)_o substrates using RF magnetron sputtering. First, a 25 nm thick epitaxial SrRuO₃ (SRO) bottom electrode layer was deposited via 90° off-axis sputtering⁴² at 600°C, followed by the growth of 1000 nm BiFeO₃ films using double-gun off-axis sputtering²³. The SrRuO₃ layer serves three purposes: it acts as a bottom electrode for out-of-plane device measurements, provides a depolarization field that orients the BiFeO₃ polarization downward, and serves as a buffer layer between the large lattice-mismatched BiFeO₃ and the substrate^{19,40}. The BiFeO₃ target used contains 5% excess Bi₂O₃ to compensate for bismuth volatility during thin-film deposition.

Device fabrication

For ferroelectric switching, a ~10 nm Pt layer was patterned into 500 μm × 200 μm devices to serve as the top electrode, while the SrRuO₃ layer served as the bottom electrode.

Ferroelectric P vs E loop measurements

Ferroelectric polarization versus applied electric field measurements were carried out using a Precision Multiferroic Ferroelectric Tester from Radiant Technologies Inc. A vertical capacitor structure of BiFeO₃ was fabricated with ~10 nm Pt as the top electrode and ~30 nm SrRuO₃ as the bottom electrode. A triangular electric pulse was applied to measure the P vs E loop, while a square electric pulse with a frequency of 10 kHz and an amplitude of 300 kV/cm was used to switch the ferroelectric polarization over many thousands of cycles.

NXMS measurements

Synchrotron X-ray diffraction measurements, including structural characterization and non-resonant X-ray magnetic scattering (NXMS), were performed on the I16 beamline at Diamond Light Source (United Kingdom)²¹, using a six-circle kappa diffractometer in reflection geometry. A 4.9 keV beam, off-resonance to all chemical elements in the sample, with a ~50 μm beam profile, was used for the NXMS measurements. A Pilatus area detector, APD, and room-temperature sample stage were used. The X-ray

beam size at the sample was adjusted to approximately $50 \mu\text{m} \times 50 \mu\text{m}$ for scanning.

Theoretical calculations

The influence of epitaxial strain on the antiferromagnetic order in the BiFeO₃ film was investigated via a thermodynamic analysis. Using order parameters describing the spontaneous polarization \mathbf{P} and the antiferromagnetic vector \mathbf{L} , an expression for the total free energy of a single ferroelectric domain was constructed. The total free energy includes four energy terms i.e., an antiferromagnetic anisotropic term, the antiferromagnetic exchange energy, the Lifshitz-type magnetoelectric coupling term and the elastic energy^{29,47}. The total free energy is given by

$$F = \int dV \left\{ K_1 (L_1^2 L_2^2 + L_2^2 L_3^2 + L_3^2 L_1^2) + K_2 L_1^2 L_2^2 L_3^2 + A \sum_{i=1}^3 (\nabla L_i)^2 + \gamma \mathbf{P} \cdot [\mathbf{L}(\nabla \cdot \mathbf{L}) - (\mathbf{L} \cdot \nabla)\mathbf{L}] + \frac{1}{2} c_{ijkl} (\varepsilon_{ij} - \varepsilon_{ij}^0) (\varepsilon_{kl} - \varepsilon_{kl}^0) \right\}$$

Where K_1 and K_2 are the antiferromagnetic anisotropy constants, A is the antiferromagnetic exchange constants, γ is the coefficient for the magnetoelectric coupling term, c_{ijkl} is the elastic stiffness tensor, ε is the epitaxial strain of the film, and ε^0 is the stress-free strain. The stress-free strain ε^0 includes the contributions from electrostriction and magnetostriction, i.e., $\varepsilon_{ij}^0 = Q_{ijkl} P_k P_l + \lambda_{ijkl} L_k L_l$, where Q_{ijkl} and λ_{ijkl} are electrostrictive and magnetostrictive coupling coefficients.

In the thermodynamic analysis, the polarization is uniform and oriented along the $(\overline{111})_{\text{pc}}$ direction, and a harmonic approximation is employed to describe the AFM order parameter in the spin cycloid⁴⁷. The relative energies of the system for the spin cycloid with different propagation directions were calculated and plotted in Figs. 1c, 1e. In the case of an isotropic compressive strain, as observed in BiFeO₃/SrTiO₃, the thermodynamically preferred directions for the spin cycloid propagation are equivalent to the unstrained case described in ref.²⁹. Consequently, the ferroelectric monodomain will have three equivalent spin cycloids \mathbf{k}_1 , \mathbf{k}_2 , and \mathbf{k}_3 associated with it, all of which are equally likely to dominate.

The calculations were repeated for a system with an anisotropic compressive strain. Reproducing the epitaxial strain state observed in BiFeO₃/NdGaO₃, where the magnitude of the compressive strain is largest along the c -axis, the breaking of symmetry leads to the lifting of the degeneracy between the three propagation directions. The \mathbf{k}_1 and \mathbf{k}_2 directions are equivalent and are less stable when compared to the \mathbf{k}_3 direction, where the total free energy is lowest. The ferroelectric monodomain in this case is therefore also expected to host a single variant of the spin cycloid.

The constructed free-energy was used to conduct phase-field simulations of both strain cases for further validation. A brief outline of the simulation setup is presented in supplementary. The simulation results corroborate the thermodynamics analysis and experimental results as shown in Fig. 3.

STEM measurements

Cross-sectional TEM lamella samples of $(111)_{\text{pc}}$ BiFeO₃ film on NdGaO₃ $(011)_o$ substrates were prepared using a dual-beam focused ion beam system (Helios G3, FEI) for interfacial anisotropic strain analysis. A thin specimen was prepared using a Ga ion beam at 30 kV, with different acceleration voltages from 5 to 1 kV for sample cleaning to minimize Ga ion damage. STEM imaging was performed using a JEM-

ARM200F (JEOL Ltd.) at the Materials Imaging & Analysis Center of POSTECH, equipped with a 5th order aberration corrector (ASCOR, CEOS GmbH) to form a 0.7 Å probe. The accelerating voltage and convergent semi-angle of the beam were 200 kV and 28 mrad, respectively. The collection semi-angles ranged from 54 to 216 mrad for high-angle annular dark-field (HAADF) imaging. Raw images were radial-difference filtered to remove background noise (Filters Lite, HREM Research Inc.). Lattice strain maps were obtained by conducting geometrical phase analysis (GPA) on high-resolution HAADF-STEM images using a GPA plug-in (HREM Research Inc.) implemented in Digital Micrograph (Gatan Inc.). Two-phase images were calculated by selecting two non-parallel reciprocal lattice vectors from the image's *Power Spectrum* to generate a 2-D strain map. The a-axis and c-axis angles were defined as 0° and 90°, respectively. The reference regions were defined in the NdGaO₃ (011)_o substrate regions with known lattice parameters.

NV diamond microscopy

Antiferromagnetic domains at the surface of BiFeO₃ films were mapped by Nitrogen Vacancy (NV) scanning microscopy from Qnami Quantum Microscope, ProteusQTM. We used parabolic tapered QuantileverTM MX+ diamond tips for their excellent signal-to-noise ratio and photon collection efficiency, making them well-suited for detecting the very small stray fields present in BiFeO₃. The NV center, consisting of a nitrogen defect and a neighboring vacancy in negative charge state (NV⁻), serves as a single-atom quantum sensor by utilizing its spin triplet state ($m_s=0, \pm 1$). In our setup, an external magnet is used to break the degeneracy of the $m_s=\pm 1$ states and a microwave (MW) source frequency is swept to obtain electron spin resonance (ESR) (between $m_s=0$ to $m_s=\pm 1$ states) which is then detected optically by measuring photoluminescence (PL) intensity. As the NV diamond tip scans the sample surface, the local stray magnetic field (B) projected along the NV- axis shifts the ESR spectra enabling the tracking of the local magnetic contrast. Here we have performed imaging in two modes namely dual iso-B and full-B. In the former, PL is measured at two MW frequencies near the FWHM of the ESR spectra and its difference (PL(v_2)-PL(v_1)) is used to generate the real space magnetic contrast. In the latter, full ESR spectra is fitted at each point and strength of local magnetic field is estimated quantitatively.

PFM measurements

Ferroelectric domains were mapped at room temperature using Piezo Force Microscopy (PFM) with a Jupiter XR Atomic Force Microscope from Oxford Instruments (Asylum Research). The Dual AC Resonance Tracking (DART) mode was used to record images by tracking the contact resonance frequency and adjusting the cantilever's drive frequency via a feedback loop. To write a domain using an electric field, the bottom SrRuO₃ layer was grounded, and the PFM tip applied the switching voltage from the top.

Acknowledgements

CBE acknowledges support for this research through a Vannevar Bush Faculty Fellowship (ONR N00014-20-1-2844), and the Gordon and Betty Moore Foundation's EPiQS Initiative, Grant GBMF9065. Ferroelectric measurement at the University of Wisconsin-Madison was supported by the US Department of Energy (DOE), Office of Science, Office of Basic Energy Sciences (BES), under award number DE-FG02-06ER46327. G.Y.K. and S.Y.C. acknowledge support from Korea Basic Science Institute (National Research Facilities and Equipment Center) Grant (2020R1A6C101A202) funded by the Ministry of

Education. S.K.O is supported by the NSF-FUSE program. R.R. acknowledges research sponsored by the Army Research Laboratory as part of the Collaborative for Hierarchical Agile and Responsive Materials (CHARM) under Cooperative Agreement Number W911NF-24-2-0100. S.S. and L.Q.C. are supported by the US Department of Energy, Office of Science, Basic Energy Sciences, under Award Number DE-SC0020145 as part of the Computational Materials Sciences Program.

Author contributions

P. P., J. S., and C. B. E. conceived the project. P. P. and J. S. carried out film growth, characterizations, and device fabrication of BiFeO₃/Pt samples. A.V., R. J., and P. G. R. performed the NXMS and synchrotron RSM measurements. S. K. O and R. R performed NV diamond microscopy and PFM imaging. S. S., F. X., and L. Q. C performed the phase field calculations. G. K and S. J. C. carried out the STEM measurements. P. P. and C.B.E. wrote the manuscript with contributions from all other co-authors. C. B. E. led the whole project.

Competing interests

The authors declare no competing interests.

Data availability

The data that support the findings of this study are available from the corresponding author on reasonable request.

References

1. Eerenstein, W., Mathur, N. D. & Scott, J. F. Multiferroic and magnetoelectric materials. *Nature* **442**, 759–765 (2006).
2. Fiebig M, Lottermoser Th, Frohlich D, Goltsev A V & Pisarev R V. Observation of coupled magnetic and electric domains. *Nature* **419**, 815–818 (2002).
3. Khomskii, D. Classifying multiferroics: Mechanisms and effects. *Physics (College. Park. Md)*. **2**, (2009).
4. Heron, J. T. *et al.* Deterministic switching of ferromagnetism at room temperature using an electric field. *Nature* **516**, 370–373 (2014).
5. Somasri, S., Meena, P., Opal, C. B. & Beaty, E. C. Temperature dependence of the crystal and magnetic structures of BiFeO₃. (1980).
6. Wang, J. *et al.* Epitaxial BiFeO₃ multiferroic thin film heterostructures. *Science (80-.)*. **299**, 1719–1722 (2003).
7. Sando, D., Barthélémy, A. & Bibes, M. BiFeO₃ epitaxial thin films and devices: Past, present and future. *J. Phys. Condens. Matter* **26**, (2014).
8. Giencke, J. E., Folkman, C. M., Baek, S. H. & Eom, C. B. Tailoring the domain structure of epitaxial BiFeO₃ thin films. *Curr. Opin. Solid State Mater. Sci.* **18**, 39–45 (2014).
9. Streiffer, S. K. *et al.* Domain patterns in epitaxial rhombohedral ferroelectric films. I. Geometry and experiments. *J. Appl. Phys.* **83**, 2742–2753 (1998).
10. F. Zavaliche, S. Y. Yang, T. Zhao, Y. H. Chu, M. P. Cruz, C. B. E. and R. R. Multiferroic BiFeO₃ films: domain structure and polarization dynamics. *Phase Transit* **79**, 991 (2006).
11. Gross, I. *et al.* Real-space imaging of non-collinear antiferromagnetic order with a single-spin magnetometer. *Nature* **549**, 252–256 (2017).
12. Sosnowska, I., Neumaier, T. P. & Steichele, E. Spiral magnetic ordering in bismuth ferrite. *J. Phys. C Solid State Phys.* **15**, 4835–4846 (1982).
13. Seidel, J. *et al.* Conduction at domain walls in oxide multiferroics. *Nat. Mater.* **8**, 229–234 (2009).
14. Chai, Y. *et al.* Voltage control of multiferroic magnon torque for reconfigurable logic-in-memory. *Nat. Commun.* **15**, 1–9 (2024).
15. Folkman, C. M., Baek, S. H. & Eom, C. B. Twin wall distortions through structural investigation of epitaxial BiFeO₃ thin films. *J. Mater. Res.* **26**, 2844–2853 (2011).
16. Saenrang, W. *et al.* Deterministic and robust room-temperature exchange coupling in monodomain multiferroic BiFeO₃ heterostructures. *Nat. Commun.* **8**, 1–8 (2017).
17. Song, C. *et al.* How to manipulate magnetic states of antiferromagnets. *Nanotechnology* **29**, (2018).
18. Baek, S. H. *et al.* Ferroelastic switching for nanoscale non-volatile magnetoelectric devices. *Nat. Mater.* **9**, 309–314 (2010).
19. Baek, S. H. *et al.* The nature of polarization fatigue in BiFeO₃. *Adv. Mater.* **23**, 1621–1625 (2011).
20. Baek, S. H. & Eom, C. B. Reliable polarization switching of BiFeO₃. *Philos. Trans. R. Soc. A*

- Math. Phys. Eng. Sci.* **370**, 4872–4889 (2012).
21. Waterfield Price, N. *et al.* Strain Engineering a Multiferroic Monodomain in Thin-Film BiFeO₃. *Phys. Rev. Appl.* **11**, 1 (2019).
 22. Weng, Y., Lin, L., Dagotto, E. & Dong, S. Inversion of Ferrimagnetic Magnetization by Ferroelectric Switching via a Novel Magnetoelectric Coupling. *Phys. Rev. Lett.* **117**, 1–6 (2016).
 23. Heron, J. T. *et al.* Electric-field-induced magnetization reversal in a ferromagnet-multiferroic heterostructure. *Phys. Rev. Lett.* **107**, 1–5 (2011).
 24. Ederer, C. & Fennie, C. J. Electric-field switchable magnetization via the Dzyaloshinskii-Moriya interaction: FeTiO₃ versus BiFeO₃. *J. Phys. Condens. Matter* **20**, (2008).
 25. Ederer, C. & Spaldin, N. A. Weak ferromagnetism and magnetoelectric coupling in bismuth ferrite. *Phys. Rev. B - Condens. Matter Mater. Phys.* **71**, 1–4 (2005).
 26. Waterfield Price, N. *et al.* Coherent Magnetoelastic Domains in Multiferroic BiFeO₃ Films. *Phys. Rev. Lett.* **117**, 1–5 (2016).
 27. Waterfield Price, N. *et al.* Electrical Switching of Magnetic Polarity in a Multiferroic BiFeO₃ Device at Room Temperature. *Phys. Rev. Appl.* **8**, 1–6 (2017).
 28. Johnson, R. D. *et al.* X-Ray imaging and multiferroic coupling of cycloidal magnetic domains in ferroelectric monodomain BiFeO₃. *Phys. Rev. Lett.* **110**, 1–5 (2013).
 29. Xue, F., Yang, T. & Chen, L. Q. Theory and phase-field simulations of electrical control of spin cycloids in a multiferroic. *Phys. Rev. B* **103**, 64202 (2021).
 30. Marti, W., Fischer, P., Schefer, J. & Kubel, F. Structure characterization with neutron powder data of LaGaO₃ and NdGaO₃ based on X-ray single-crystal data: Evidence for an inversion center. *Zeitschrift für Krist. - New Cryst. Struct.* **211**, 891–894 (1996).
 31. Ou, Z. *et al.* Strong Electron-Phonon Coupling Mediates Carrier Transport in BiFeO₃. *Adv. Sci.* **10**, 1–9 (2023).
 32. Zhong, H. *et al.* Quantitative Imaging of Exotic Antiferromagnetic Spin Cycloids in BiFeO₃ Thin Films. *Phys. Rev. Appl.* **17**, 1 (2022).
 33. Taylor, J. M. *et al.* High-sensitivity diamond magnetometer with nanoscale resolution. *Nat. Phys.* **4**, 810–816 (2008).
 34. Meisenheimer, P. *et al.* Switching the spin cycloid in BiFeO₃ with an electric field. *Nat. Commun.* **15**, 1–8 (2024).
 35. Maletinsky, P. *et al.* A robust scanning diamond sensor for nanoscale imaging with single nitrogen-vacancy centres. *Nat. Nanotechnol.* **7**, 320–324 (2012).
 36. Dufour, P. *et al.* Onset of Multiferroicity in Prototypical Single-Spin Cycloid BiFeO₃ Thin Films. *Nano Lett.* **23**, 9073–9079 (2023).
 37. Ramazanoglu, M. *et al.* Local weak ferromagnetism in single-crystalline ferroelectric BiFeO₃. *Phys. Rev. Lett.* **107**, 1–5 (2011).
 38. Meyer, S., Xu, B., Verstraete, M. J., Bellaiche, L. & Dupé, B. Spin-current driven Dzyaloshinskii-Moriya interaction in multiferroic BiFeO₃ from first principles. *Phys. Rev. B* **108**, 24403 (2023).

39. Echeverría-Alar, S. & Clerc, M. G. Labyrinthine patterns transitions. *Phys. Rev. Res.* **2**, 1–5 (2020).
40. Zhong, H. *et al.* Quantitative Imaging of Exotic Antiferromagnetic Spin Cycloids in BiFeO₃ Thin Films. *Phys. Rev. Appl.* **17**, 1 (2022).
41. Finco, A. *et al.* Imaging Topological Defects in a Noncollinear Antiferromagnet. *Phys. Rev. Lett.* **128**, 1–6 (2022).
42. Meisenheimer, P. *et al.* Designed spin-texture-lattice to control anisotropic magnon transport in antiferromagnets. **2404639**, 1–8 (2024).
43. Mangeri, J. *et al.* Coupled magnetostructural continuum model for multiferroic BiFeO₃. *Phys. Rev. B* **108**, (2023).
44. Yang, T. *et al.* The Evidence of Giant Surface Flexoelectric Field in (111) Oriented BiFeO₃ Thin Film. *ACS Appl. Mater. Interfaces* **9**, 5600–5606 (2017).
45. Hsieh, Y. H. *et al.* Permanent ferroelectric retention of BiFeO₃ mesocrystal. *Nat. Commun.* **7**, 1–9 (2016).
46. Husain, S. *et al.* Non-volatile magnon transport in a single domain multiferroic. *Nat. Commun.* **15**, 1–9 (2024).
47. Sando, D. *et al.* Crafting the magnonic and spintronic response of BiFeO₃ films by epitaxial strain. *Nat. Mater.* **12**, 641–646 (2013).

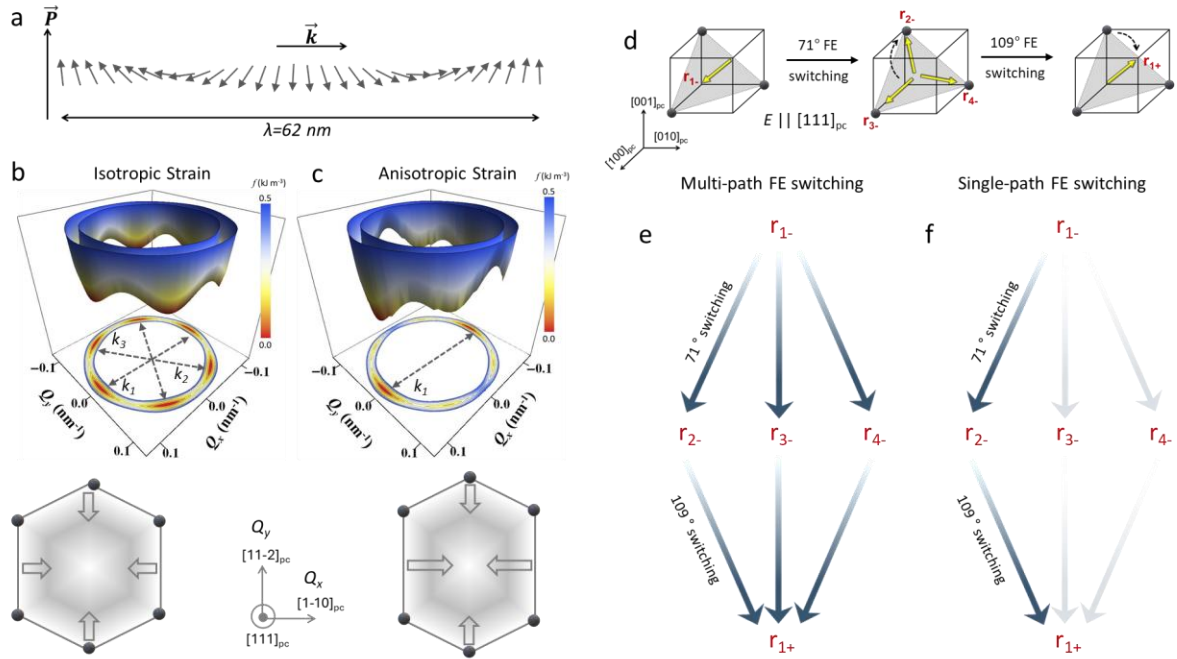


Fig. 1. Anisotropic strain-engineered AFM monodomain with deterministic switching. **a.** Schematic illustration of the spin cycloid in BiFeO₃, showing its alignment within the plane of polarization and propagation vector k . **b.** Thermodynamic simulation under isotropic compressive strain of 0.95% (e.g., SrTiO₃) along both $[1-10]_{pc}$ and $[11-2]_{pc}$ directions with the corresponding 3D polar plot of the calculated free energy vs. the spin cycloid direction. In this case, all three antiferromagnetic domains are degenerate. **c.** Similar calculations considering anisotropic compressive strain, 2.5% along $[1-10]_{pc}$ and 2% along $[11-2]_{pc}$ directions (e.g., NdGaO₃) which stabilizes only one variant of type I spin cycloid. **d.** Schematic representation of multi-stage ferroelectric switching in $[111]_{pc}$ BiFeO₃. **e.** The presence of equally favorable multi-path 71° switching in isotropically strained BiFeO₃ (e.g., SrTiO₃), leading to the formation of charged domain walls and polarization fatigue. **f.** Hypothesis of anisotropic strain-controlled fatigue-free ferroelectric switching via a preferred switching path (e.g. in NdGaO₃).

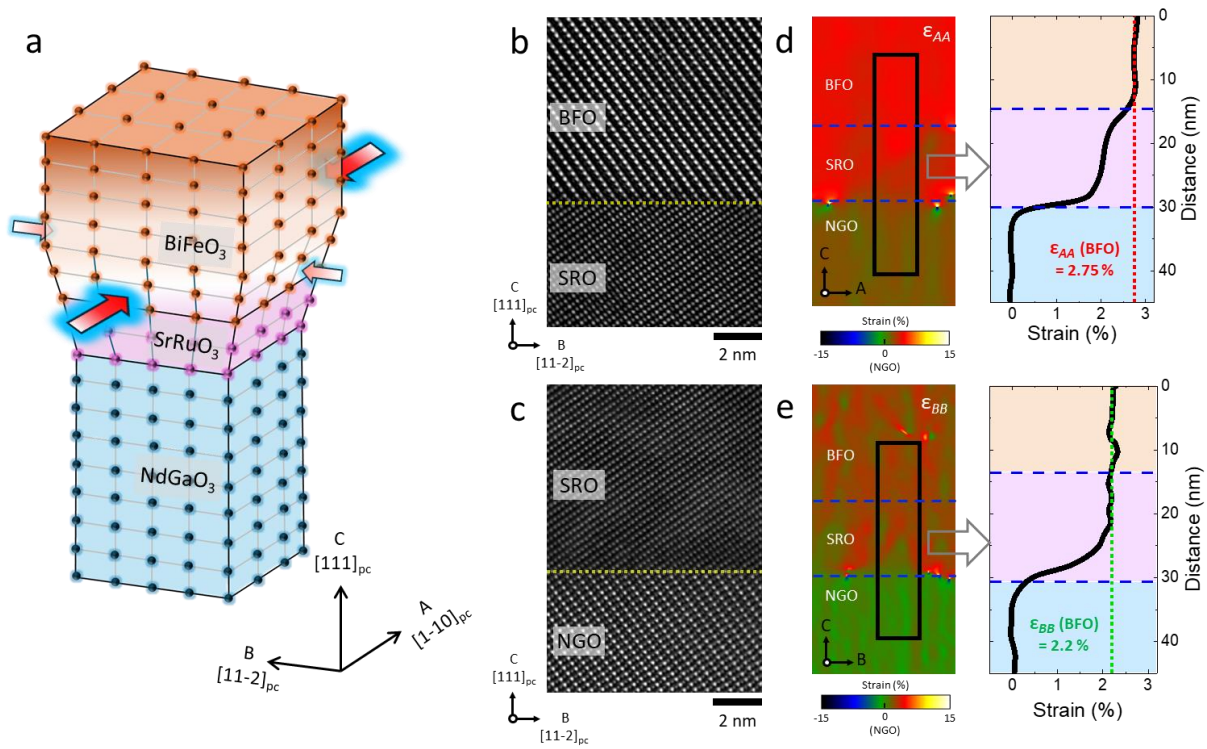


Fig. 2. High-quality (111)_{pc} BiFeO₃ thin film with anisotropic in-plane strain. **A.** Schematic representation of the BiFeO₃ film showing anisotropic strain between A ([1-10]_{pc}) and B ([11-2]_{pc}) directions near the interface. **b-c.** Cross-sectional high-resolution HAADF-STEM images along the [1-10]_{pc} zone axis, revealing atomically sharp interfaces. **d-e.** In-plane lattice strain maps (ε_{AA} and ε_{BB}) and line profiles at the BiFeO₃/SrRuO₃/NdGaO₃ interface along the B and A projections, respectively. The in-plane lattice strain maps were calculated from HAADF-STEM images in Fig S6b and c. In the line profiles, the red and green lines represent the lattice strain values of BiFeO₃ layers for each projection direction. The intensity profiles indicate that the initial BiFeO₃ layer is anisotropically strained, with greater strain along the A ([1-10]_{pc}) direction.

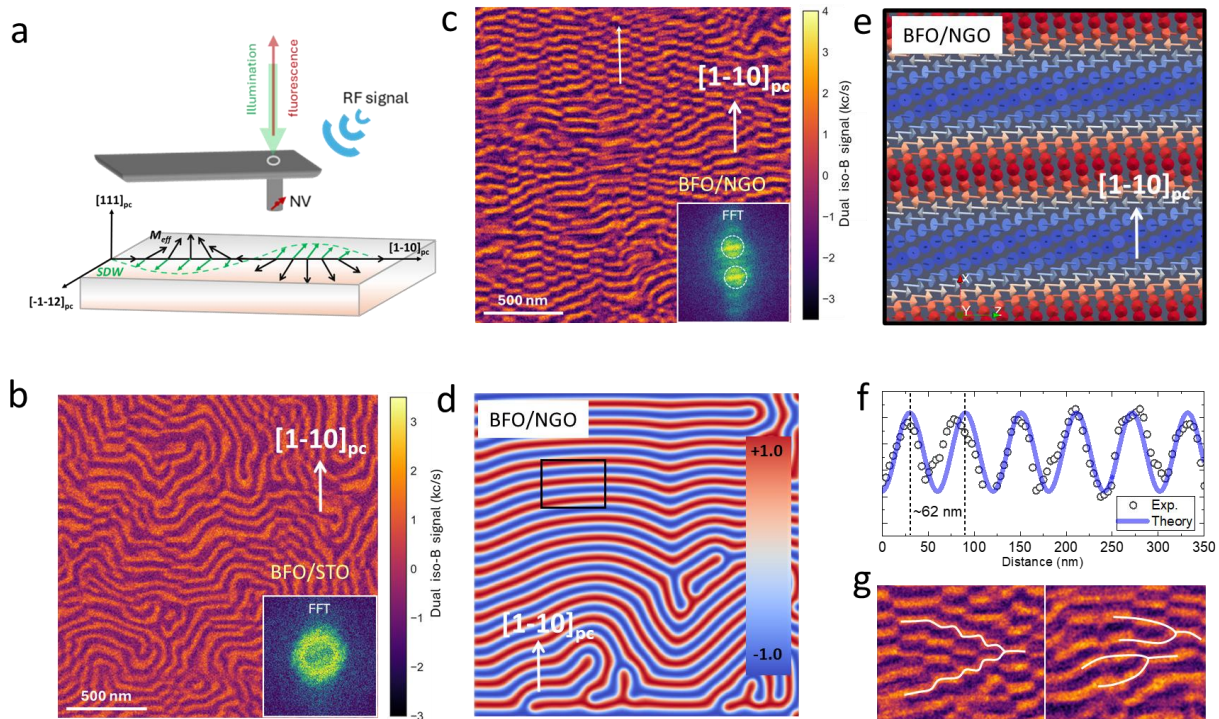


Figure 3. Real space imaging of antiferromagnetic domains. **a.** Schematic illustration of scanning NV diamond microscope setup used to probe the periodic modulation of stray magnetic field. **b.** Corresponding microscope image of as-grown BiFeO₃ films on (111) SrTiO₃, showing a complex pattern. **c.** Similar image for BiFeO₃ on (011)_o NdGaO₃ substrate, displaying a very ordered pattern, indicating the presence of multiple antiferromagnetic domains on SrTiO₃ and a single antiferromagnetic domain on NdGaO₃. **d.** Thermodynamic phase field simulation of the magnetic domain mapping of BiFeO₃ film on NdGaO₃. **e.** Estimation of the spin-cycloid periodicity from a section profile of the image in **c**, which matches excellently with theoretical data. **f.** Estimation of the spin-cycloid periodicity from a section profile of the image in **c**, which matches excellently with theoretical data. **g.** A close-up of the NV image in **c**, showing intriguing patterns likely originating from topological defects.

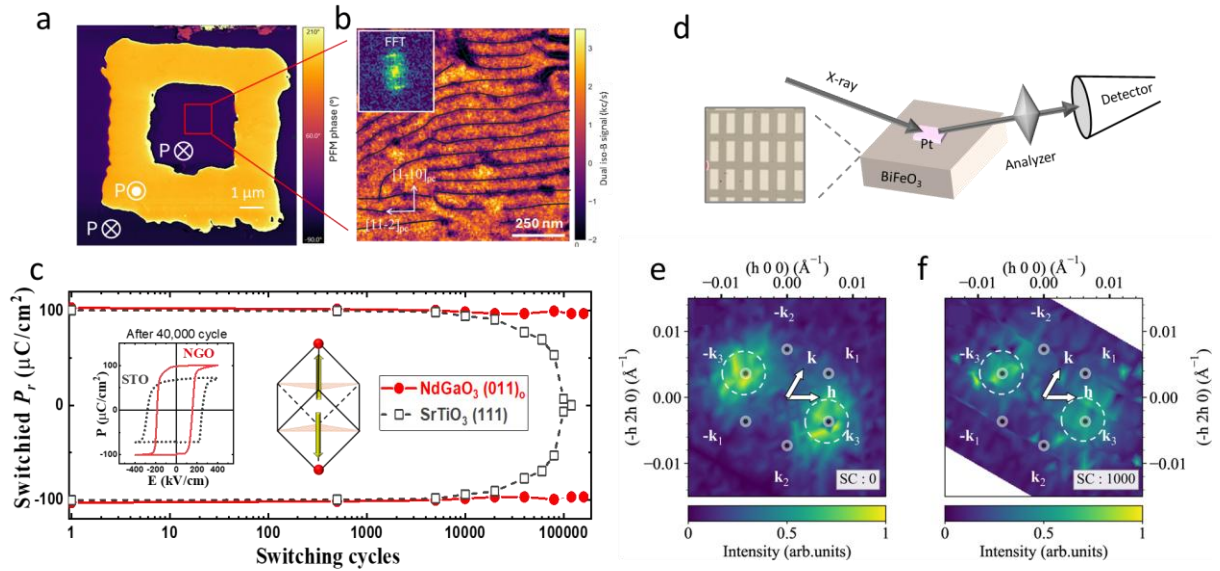


Figure 4. Deterministic electric field switching. **a.** PFM switching and electric field writing of a box-in-a-box pattern. **b.** Corresponding NV microscopy image of the inside region after complete switching cycle, clearly showing the presence of a robust spin cycloid. **c.** Ferroelectric fatigue measurement data for the BiFeO₃ film on NdGaO₃ (011)_o, obtained using a square electric field pulse with an amplitude of 300 kV/cm and a frequency of 10 kHz. The inset in **c** shows the ferroelectric polarization data after 40,000 switching cycles. **d.** Schematic illustration of the NXMS setup for ferroelastic and antiferromagnetic domain mapping. **e.** NXMS scan near the (009)_h reflection (which is specific to magnetic domain mapping) on the as-grown BiFeO₃ film on NdGaO₃ (011)_o, revealing a single antiferromagnetic domain. **f.** Corresponding NXMS scans after 1,000 cycles of ferroelectric polarization switching. Notably, the antiferromagnetic domains exhibit single-domain characteristics, highlighting their robustness.